



# Numerical simulation of powder flow during spreading in additive manufacturing

Wenguang Nan<sup>a,b</sup>, Mojtaba Ghadiri<sup>b,\*</sup>

<sup>a</sup> School of Mechanical and Power Engineering, Nanjing Tech University, Nanjing 211816, China

<sup>b</sup> School of Chemical and Process Engineering, University of Leeds, Leeds LS2 9JT, UK

## ARTICLE INFO

### Article history:

Received 8 August 2018

Received in revised form 11 October 2018

Accepted 27 October 2018

Available online 29 October 2018

### Keywords:

Additive manufacturing

Particle spreading

Sintering

Discrete element method

Shear band

Mass flow rate.

## ABSTRACT

Additive manufacturing (AM) has attracted increasing attention in a wide range of applications, due to its ability for rapid manufacturing of complex shapes directly from a Computer-Aided Design (3D CAD) output. One of the manufacturing methods is based on powder processing, where a thin bed is formed to which an energy beam is applied to sinter and melt the powder. A major bottleneck in this method is associated with powder spreading, as its dynamics is sensitive to powder properties, machine design and operation conditions, such as speed of spreading. The effects of gap height and blade spreading speed on the evolving shear band and mass flow rate through the gap have been simulated by Discrete Element Method, using the most realistic physical and mechanical properties of the particles. It is shown that the particle velocity in the powder heap in front of the blade could well be described by a universal curve given by the Gauss error function. The mass flow rate through the gap increases linearly with the gap height. There exist two flow regimes with the increase of the blade spreading speed. Initially, the mass flow rate has a linear dependence on the blade speed, but eventually approaches an asymptotic value, implying a limit beyond which the mass flow rate cannot be further increased. This has an important implication on the speed of spreading.

© 2018 Elsevier B.V. All rights reserved.

## 1. Introduction

Additive manufacturing (AM) is paving the way towards the next industrial revolution [1–3]. AM creates three-dimensional (3D) objects by stepwise layer-by-layer approaches which are controlled by a digital model. This unique feature allows the production of complex or customized parts directly from the Computer-Aided Design (3D CAD) output, without the need for expensive tooling such as punches, dies or casting moulds and the assembling of multiple components [4–12]. It also reduces the need for many conventional processing steps and eliminates most of the constraints that hinder optimal design, creativity and ease of manufacturing of complex parts. Therefore, AM is going through an exponential growth and is being widely used as a novel production technology for the design and manufacturing of high-performance components in the aerospace, biology, medical and energy applications [5,7]. For example, complex fuel injector nozzles in aerospace technology which previously required assembly of multiple parts can now be directly fabricated by AM with lightweight engineered structures, resulting in significant cost savings.

Among several manufacturing methods, the powder-based process has attracted increasing attention due to its flexibility [11,13]. In this

process, typically 10–50  $\mu\text{m}$  particles are spread over a work surface made of particles, which are already partially sintered/melted, by a roller or blade, resulting in a particle layer with a thickness of a few particle diameters. Then a laser or electron beam is shone onto it to melt the specified area. Once a cross-section is scanned, the work surface is lowered and the process is repeated until the completion of the production. The powder spreading process has an important effect on the quality of the powder bed for subsequent sintering/melting, which in turn influences the characteristics and quality of the final product [4,5]. Poor powder flow during spreading causes variations in the solid volume fraction of the particle layer and roughness of its surface, leading to weak bonding between layers or formation of cavities, producing inferior products with poor mechanical performance [14–16]. Lack of sufficient understanding of the powder dynamics, such as the factors which influence the powder flow rate through the spreader gap, hinders further refinement of this technology and introduction of new materials.

Recently, the Discrete Element Method (DEM) has been used to describe the mechanical behaviour of the powder spreading system in additive manufacturing [17–21]. Parteli and Pöschel [17] and Haeri et al. [18] studied the effect of spreading speed and gap height on the bed quality in the roller spreading system, and showed that high spreader translational velocity could lead to low bed quality. Chen et al. [19] used spherical particles with tuned mechanical properties

\* Corresponding author.

E-mail address: [M.Ghadiri@leeds.ac.uk](mailto:M.Ghadiri@leeds.ac.uk) (M. Ghadiri).

and found that the effects of the blade spreading speed and gap height on the dynamic repose angle of the heap in front of the blade were negligible. Haeri [20] explored the effect of the blade geometry on the spreading performance, and found that the bed quality could be improved by using a super-elliptic edge profile for the spreader. These works also showed that the powder spreading process was very sensitive to powder properties (including particle size distribution, interfacial surface energy, sliding friction coefficient and so on) and operation conditions (including spreading speed and gap height). Nan et al. [21] characterised all the relevant physical and mechanical properties of gas-atomised 316 L stainless steel particles and used them in numerical simulations of powder spreading by a blade. They showed that transient jamming occurred in narrow spreader gaps and was manifested by the formation of empty patches over the work surface. They also analysed the frequency and period of jamming and established their relationships with particle properties, gap height and spread speed. The factors which have not been analysed in detail so far are the powder flow rate through the spreader gap as influenced by the spreader speed, as well as the shear zone in the heap in front of the blade which is responsible for controlling of the powder flow rate. They are directly related to the issues during powder spreading, such as the criterion for the maximum spreading throughput, and the empty patches caused by the particle jamming for small spreading gaps.

In this work, the particle flow in the blade spreading process is simulated by Discrete Element Method. The particle heap comprises gas-atomised stainless 316 L steel particles. It is subjected to a translational motion by a vertical blade with a gap allowing a thin particle layer to be spread. The effects of the gap height and blade spreading speed on the shear zone of the particle heap in front of the blade and the resulting mass flow rate through the gap are analysed. This provides a benchmark for the maximum speed of the spreader, an influential factor controlling the production throughput.

## 2. Method

Gas-atomised 316 L stainless steel particles, provided by Sandvik Osprey Ltd., Neath, UK, are modelled in this work. The characterisation of their physical and mechanical properties have been done by Nan et al. [21], including the size and shape distributions, hardness and Young's modulus, interfacial surface energy, coefficients of restitution and sliding friction. The particles have a size distribution in the range 15–55  $\mu\text{m}$ , for which the number based  $D_{10}$ ,  $D_{50}$  and  $D_{90}$  are 20  $\mu\text{m}$ , 32  $\mu\text{m}$  and 45  $\mu\text{m}$ , respectively. To describe the dynamics of particle flow in the spreading process, the particles are modelled as discrete entities and their motions are tracked individually by solving Newton's laws of motion [22–24], for which the EDEM™ software package provided by DEM Solutions, Edinburgh, UK, is used.

### 2.1. Discrete element method

According to the DEM, originally proposed by Cundall and Strack [22], the movement of an individual particle is described by the translational and rotational motions:

$$m_i \frac{d\mathbf{v}_i}{dt} = \sum \mathbf{F}_{c,i} + m_i \mathbf{g} \quad (1)$$

$$\frac{d(\mathbf{I}_i \cdot \boldsymbol{\omega}_i)}{dt} = \mathbf{R}_i \cdot \sum \mathbf{M}_{c,i} \quad (2)$$

where  $m_i$ ,  $\mathbf{I}_i$ ,  $\mathbf{v}_i$  and  $\boldsymbol{\omega}_i$  are the mass, moment of inertia, translational velocity and angular velocity, respectively;  $\mathbf{F}_{c,i}$  is the contact force, originating from its interaction with neighbouring particles or walls;  $\mathbf{M}_{c,i}$  is the contact torque, arising from the tangential and normal contact forces;  $\mathbf{R}_i$  is the rotation matrix from the global to the local coordinate

system in which the calculation of the rotation expressed by Eq. 2 is accomplished.

As introduced by Favier et al. [25], the non-spherical particles are described by the overlapping multi-sphere model, as shown in Fig. 1. Thus, the interactions between any two non-spherical particles can be simplified as that of spherical particles. In this work, the elastic contact force is described by Hertz-Mindlin contact model [23], and the adhesive interaction is accounted for by JKR theory [26]:

$$F_{JKR} = 4\sqrt{\pi\gamma E^*} a^{3/2} \quad (3)$$

where  $\gamma$  is the surface energy;  $E^*$  is the equivalent Young's modulus;  $a$  is the contact radius. More features and further information of the simulation method are given by Nan et al. [21] and not shown here for brevity.

### 2.2. Simulation conditions

The simulation system comprises a spreading blade and a base, as shown in Fig. 2, where  $D$  represents the characteristic size  $D_{90}$  by number. The dimensions of the simulation domain in the spreading and lateral directions are  $400D$  and  $10D$ , respectively. The front and rear boundaries (i.e. in the  $Y$  direction) are treated as periodic boundaries for particle flow. The base with the same length and width as of the simulation domain is made up of clumped cylinders with axes along the  $Y$  direction, where the cylinder diameter is equal to  $D$  and the distance between adjacent cylinder centres is equal to  $0.5D$ . In this arrangement, the bulk sliding of the particles on the base is mitigated by the fully-rough wall. The blade with the same width of the base has a thickness of  $4D$  in the spreading direction, and its height is much larger than that of the initial particle bed.

The initial particle bed is prepared by using the poured packing method, where approximately 16,000 particles are generated. These particles have a size distribution in the range 15–55  $\mu\text{m}$ , and are classified into four main size classes based on the equivalent-circle diameter of the projected area. The number frequency for the size classes of 15–25  $\mu\text{m}$ , 25–35  $\mu\text{m}$ , 35–45  $\mu\text{m}$  and 45–55  $\mu\text{m}$  are 29.6%, 40.8%, 23.9% and 5.7% [21], respectively. For each size class, 5–10 particles are randomly selected for simulating their shapes, with a total of 24 types of shape used in the simulation, as shown in Fig. 1. The physical and mechanical properties of particles, as needed for numerical simulations are given in Table 1. They are characterised by special methods and have been described in the previous work [21]. The integration time step is  $10^{-8}$  s. At the start of the simulation, the blade is lifted vertically to the specified position, forming a vertical gap  $\delta$  between the spreading blade and layering base. It is then moved along the  $X$  direction with a constant velocity  $U$ , by which the particles are spread. To evaluate the effect of spreading conditions on the particle flow in the spreading process, the gap  $\delta$  is varied from  $1.5D$  to  $4.0D$ , and the blade speed  $U$  is varied from 0.01 m/s to 0.16 m/s.

## 3. Simulation results

### 3.1. Shear band

As the particle bed is subjected to the horizontal motion of the blade, a shear band is locally formed around the blade. Here, the region 'in front of the blade' is shown in Fig. 3. Its dimensions are  $10D$  in the  $Y$  direction,  $2.5D$  in length, in the  $X$  direction, and  $6D$  in height, in the  $Z$  direction. It is divided into 11 bins in the  $Z$  direction with a height equal to  $D$ , and the adjacent bins overlap in height by 50%. This is done to get a smooth velocity profile. As the blade moves in the  $X$  direction, only the component of particle velocity in this direction  $u_x$  is considered, and it is normalised by the blade speed  $U$ .

The profile of  $u_x$  along the vertical direction is shown in Fig. 4, where the blade speed is 0.04 m/s. The particle velocity  $u_x$  increases with the bin centre position  $H$  and reaches a plateau when  $H$  is larger than  $H_1 = \delta + D$ . This trend suggests that the effect of blade shearing on the

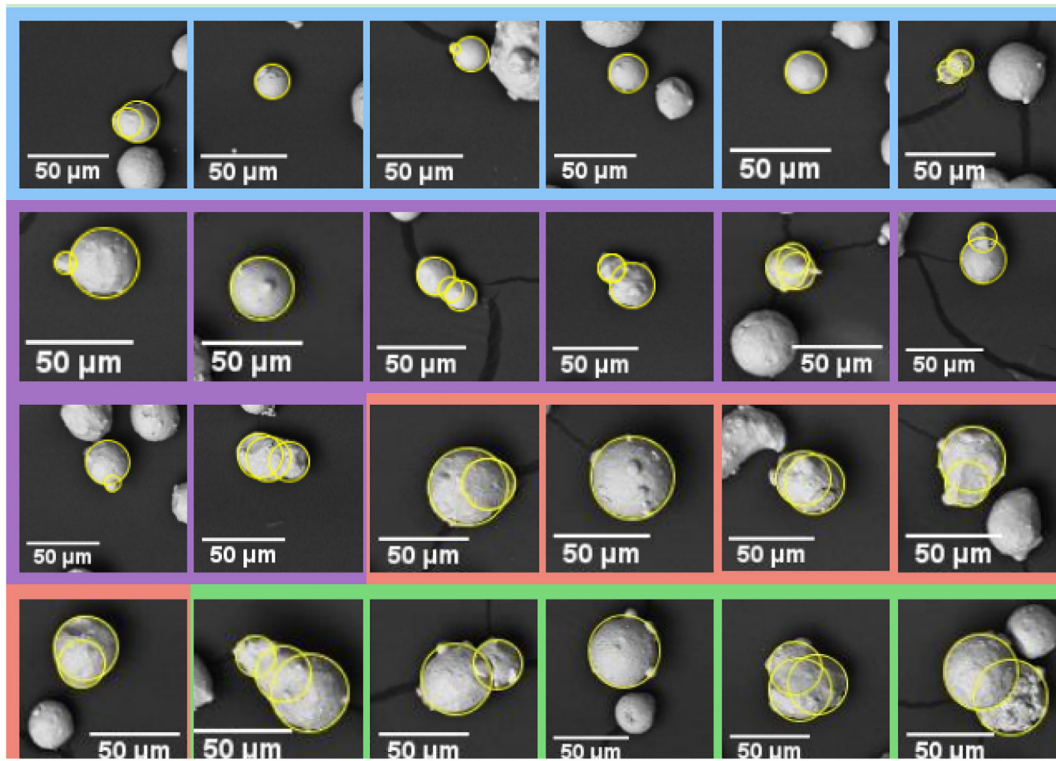


**Fig. 1.** Particle shapes used in DEM simulations; each size and shape class are housed in a box with coloured borders, as shape varies with size; six blue boxes (15–25  $\mu\text{m}$ ), eight purple boxes (25–35  $\mu\text{m}$ ), five red boxes (35–45  $\mu\text{m}$ ), and five green boxes (45–55  $\mu\text{m}$ ).

particles mainly takes place in the zone with  $H \leq \delta + D$ . For a small gap height (i.e.  $\delta/D = 1.5$ ), the shear band centre position for  $u_x/U = 0.5$  is very close to the base, and the shear zone is not fully developed near the base, resulting in a large particle velocity at  $H/D = 0.5$ . With the increase of the gap height, the profiles move to the right, and the velocity of particles closest to the base decreases significantly, due to further developing of the shear zone near the base. When the gap height is increased to  $\delta/D = 4.0$ , the shear band is fully developed, resulting in a sigmoidal shape profile of particle velocity.

Profiles of  $u_x$  for other blade speeds are all similar to the ones shown in Fig. 4. By rescaling of the bin centre position  $H$  in terms of  $(H - h_c)/h_w$ , where  $h_c$  is the shear band centre position in the vertical direction with respect to the base and  $h_w$  is a linear function of the shear band width,  $w$ , acting as a scale factor. These profiles (i.e. totally 32 cases) all collapse

onto a universal curve, as shown in Fig. 5. This curve is well fitted by the Gauss error function which is denoted by “erf”:

$$\frac{u_x}{U} = 0.5 \left[ 1 + \operatorname{erf} \left( \frac{H - h_c}{h_w} \right) \right] \quad (4)$$

Thus, the profile of particle velocity could be completely described by the centre position and widths of the shear band.

The variation of the shear band centre position  $h_c$  with the blade speed is shown in Fig. 6. With the increase of blade speed, the shear band centre position moves to a lower vertical position. The shear band centre position is more sensitive to the blade speed for larger gap heights. With the increase of gap height, the shear band centre position moves to higher vertical positions, which agrees well with the

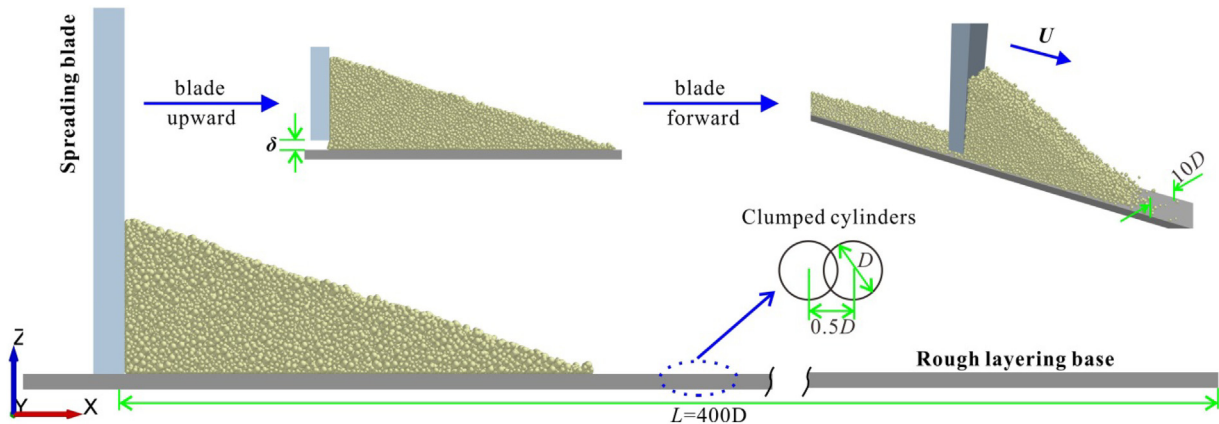


**Fig. 2.** Schematic of particle spreading process for simulation [21].



**Table 1**  
Particle properties in the simulation.

Parameters	Value
Particle diameter, $D$ (mm)	0.045
Particle density, $\rho$ (kg/m <sup>3</sup> )	7980
Young's modulus, $E$ (GPa)	2.1
Poisson ratio, $\nu$	0.3
Friction coefficient, $\mu$	0.5
Restitution coefficient, $e$	0.64
Surface energy, $\gamma$ (mJ/m <sup>2</sup> )	1.4

results shown in Fig. 4. The difference between the shear band centre positions for different gap heights decreases with the blade speed. This suggests that the shear band centre position is less affected by the gap height at large blade speed.

Here, the positions where  $u_x/U = 0.05$  and  $u_x/U = 0.95$  are regarded as the lower and upper boundaries of the shear band. Thus, the shear band width,  $w$ , is calculated from the distance between these two extreme positions, and is equal to  $2.5h_w$ , due to  $0.5(1 + \text{erf}(-1.25)) = 0.05$  and  $0.5(1 + \text{erf}(1.25)) = 0.95$  in Eq. (4). The variation of the shear band width  $w$  with the blade speed is shown in Fig. 7. For small blade speeds, the shear band width fluctuates with the increase of gap height. For example, when the blade speed is between 0.04 m/s and 0.08 m/s, the shear band width is around  $3.0\text{--}3.5D$ , which is also about  $4.0\text{--}4.7D_v$ , as  $D = 1.35D_v$ . As the blade speed is increased to 0.10 m/s and beyond, the shear band width increases almost linearly with the gap height.

### 3.2. Mass flow rate through the gap

As the particle bed is sheared by the blade, particles with smaller  $u_x$  than the blade are deposited onto the base through the gap. The mass flow rate is unsteady, due to the discontinuous nature of particle flow in narrow openings. When the gap height is small (i.e.  $\delta/D = 1.5$ ), the transient mass flow rate could even be zero, due to the particle jamming, which has been discussed in detail by Nan et al. [21]. Here, the mass flow rate is time-averaged and normalised by dividing it by  $\rho WD$ , where  $\rho$  is particle density,  $W$  is the width of the base in the lateral direction ( $Y$  direction), and  $D$  is  $D_{90}$  of particle size number distribution.

Variations of the mass flow rate with the blade speed are shown in Fig. 8(a). At low blade speeds, the mass flow rate increases linearly with the blade speed, and its slope increases with the gap height. At large blade speeds, there is a change in the trend and the mass flow rate increases to an asymptotic value, which depends on the gap height. This trend suggests that the spreading throughput is limited at large spreading speeds. There are therefore two flow regimes, one dependent and another independent of the blade speed. It appears that the blade speed corresponding to the flow regime transition is not affected by

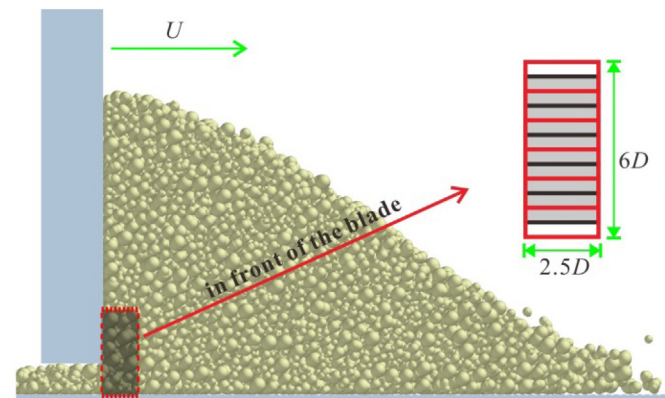


**Fig. 3.** Illustration of the heap region 'in front of the blade'.

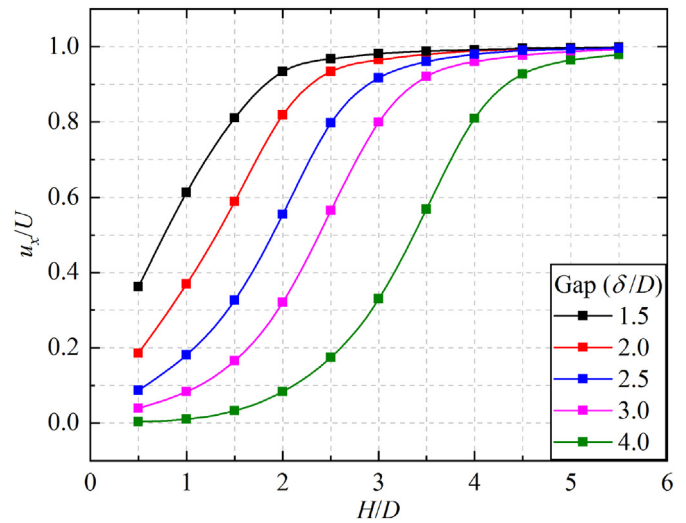


**Fig. 4.** Particle velocity profiles in the region 'in front of the blade' for different gap heights for blade speed of 0.04 m/s.

the gap height. This will be probed in more detail below. The variation of mass flow rate with the gap height is shown in Fig. 8(b), for which a linear relationship with the gap height is observed. The slope depends on the blade speed. Thus, the following functional form is proposed for the mass flow rate:

$$Q = \rho f_U W (\delta - \delta_c) \quad (5)$$

where  $\delta_c$  is the critical gap height at which the mass flow rate is zero, namely the intercept on the abscissa in Fig. 8(b).  $\delta_c$  accounts for the boundary effects of the blade front tip, resulting in an effective gap height of  $\delta - \delta_c$ . The dependency of the slope of the line on the blade speed is expressed by  $f_U$  for the linear flow regime.

The variation of  $f_U$  with the blade speed is shown in Fig. 9(a). At low blade speeds  $U$ ,  $f_U$  increases linearly with  $U$  with a slope of about 0.55. At large blade speeds,  $f_U$  increases gradually to a plateau around 0.043. Fig. 9(a) also shows there exists a critical blade speed,  $U_c$ , above which the mass flow rate is almost independent of the blade speed. It is around 0.1 m/s for the particle system here. The critical gap height  $\delta_c$  as a function of the blade speed is shown in Fig. 9(b). Its value is around  $D$  (i.e.  $1.35D_v$ , where  $D_v$  is the arithmetic mean volume equivalent diameter) for the speed range 0.04–0.1 m/s, which is commonly used. In the case

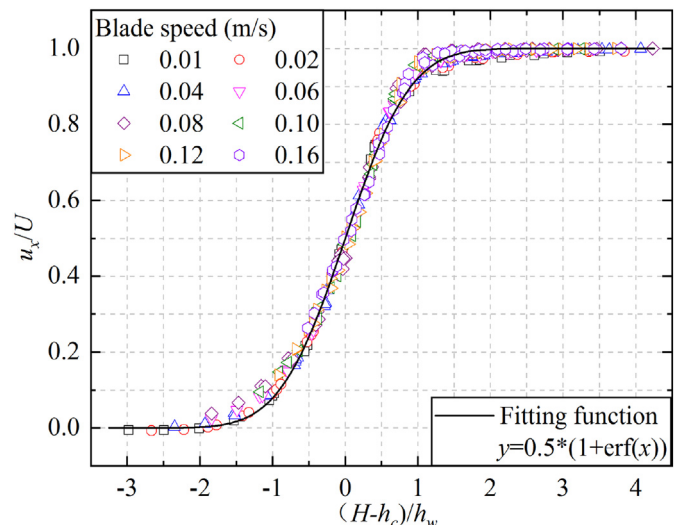


**Fig. 5.** Universal curve for the particle velocity profile in the region 'in front of the blade'.

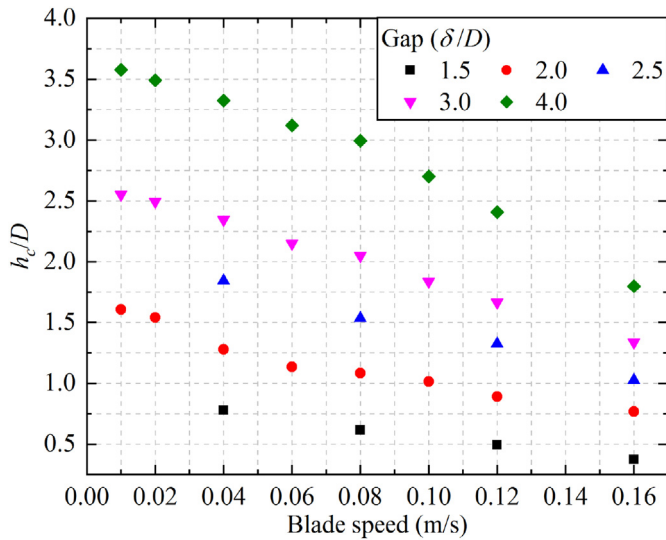


Fig. 6. Variation of the shear band centre position  $h_c$  with respect to the spread layer surface with the blade speed for different gap heights.

here, the critical gap height is caused by one side wall moving and the other being stationary, whilst the two side walls in the wedge-shaped hoppers are stationary [27–30]. Thus, the critical gap size in this work is smaller than that in hopper flow. Fig. 9 also suggests that even in the ideal case where the particles are uniformly spread onto the base without jamming, the gap height should be at least  $2D$  to cover the base without any empty patches.

The critical blade speed could also be examined by comparing the gravity inertial timescale  $t_g$  and spreading inertial timescale  $t_s$ , which are defined as.

$$t_g = \sqrt{D/g} \quad (6)$$

$$t_s = D/U \quad (7)$$

The gravity inertial timescale  $t_g$  is the time taken by a particle with zero initial velocity to fall a distance of  $D/2$  under gravity acceleration  $g$ , whilst the spreading inertial timescale  $t_s$  is the time taken by the blade with velocity  $U$  to pass over a static particle with  $D$ . If the spreading inertial timescale is much less than the gravity inertial timescale, i.e.  $t_s = t_g/k$  ( $k > 1$ ), the gravity effect on the spreading process could be

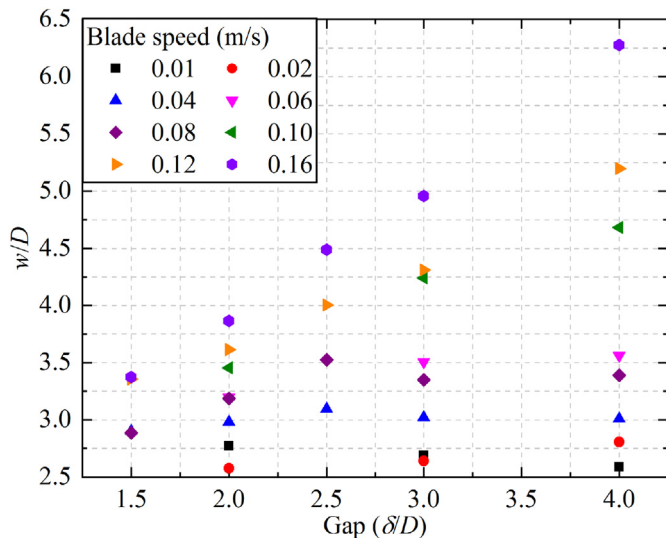


Fig. 7. Variation of the shear band width  $w$  with the gap height for different blade speeds.

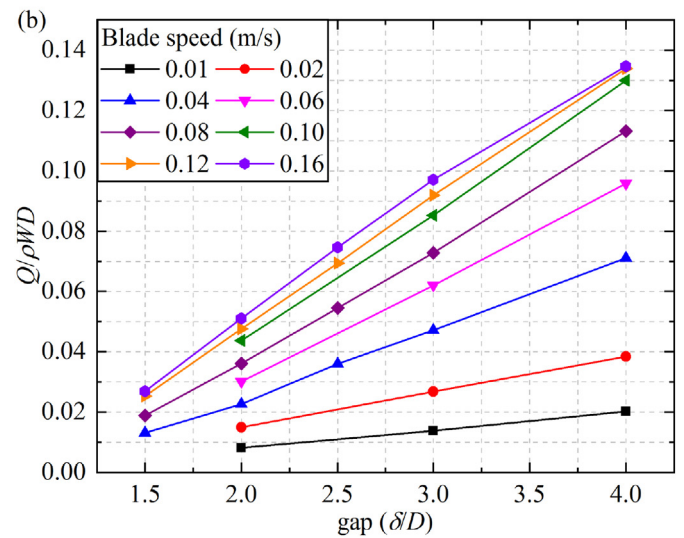
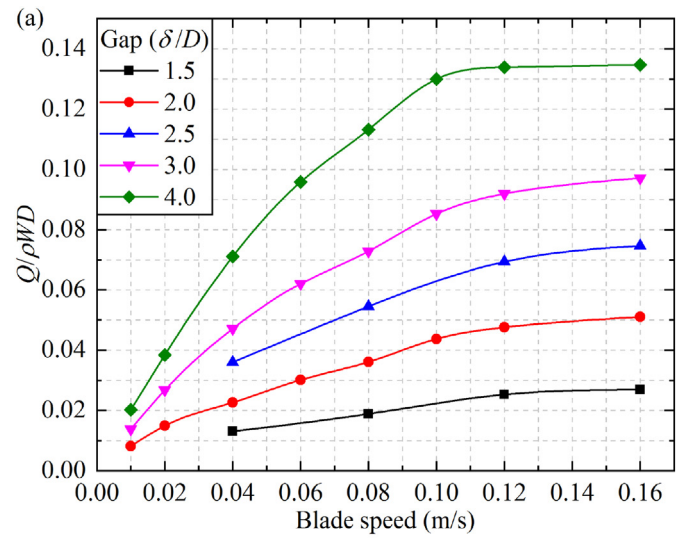


Fig. 8. Variation of mass flow rate with (a) blade speed and (b) gap height.

limited, and the particles do not have enough time to fall down to fill the dilated zone caused by the blade shearing. This could also be observed from the vertical velocity of particles in front of the blade in Fig. 3, as shown in Fig. 10. When the blade speed is 0.1 m/s or greater, the falling velocity of particles (i.e.  $-u_z$ ) does not show any further increase with the increase of  $U$ , indicating that no more additional particles could move to the dilated zone as the blade speed is increased. Therefore, by comparing  $t_s$  and  $t_g$ , a critical blade speed could be defined as:

$$U_c = k\sqrt{gD} \quad (8)$$

where  $k$  is the ratio of the two timescales ( $> 1$ ). The variation of the critical blade speed with  $k$  is shown in Table 2. In this work,  $k = 5$  gives the same critical blade speed (i.e. 0.1 m/s) as given in the description of Figs. 8 and 9. Therefore, the critical blade speed is well described by Eq. (8).

#### 4. Conclusions

The particle spreading process in additive manufacturing has been analysed by DEM simulations, using realistic physical and mechanical properties of particles as measured for single particles in the previous work. The effect of the spreading process on the particle flow has been

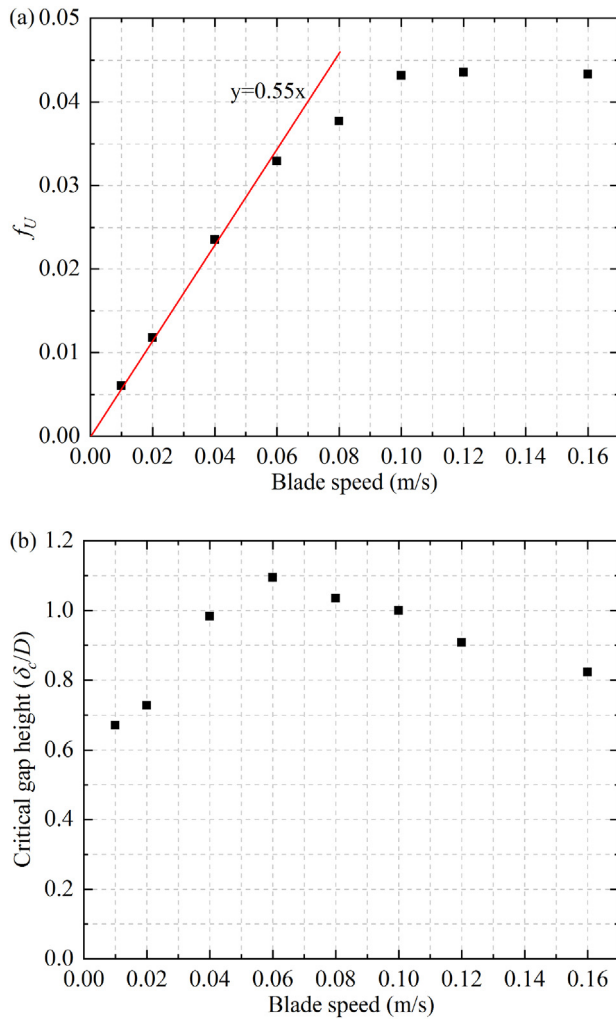


Fig. 9. Variation of (a)  $f_U$  and (b) critical gap height with blade speed.

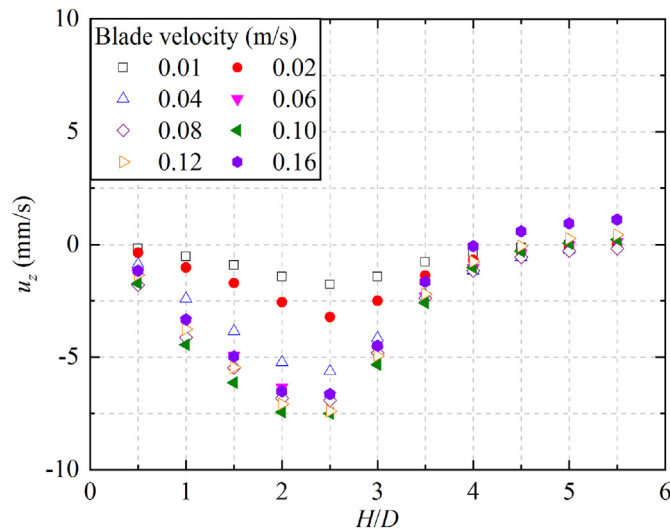


Fig. 10. Profiles of  $u_z$  in the heap in front of the blade for different blade speeds for the gap height of  $\delta/D = 3.0$ .

analysed in terms of the shear band and mass flow rate through the gap height. The main results from the present study are summarised as follows:

Table 2

Variation of critical blade speed with  $k$ .

$k$	3	4	5	6	7
$U_c$ (m/s)	0.063	0.084	0.105	0.126	0.147

- 1) The velocity profiles of particles in the heap in front of the blade follow a universal curve given by the Gauss error function. With the increase of blade speed or the decrease of the gap height, the shear band centre moves to lower vertical positions.
- 2) The mass flow rate through the gap increases linearly with the gap height. There is a critical size of about  $D$  below which there is no flow. The dependence of the mass flow rate on the blade speed is more complex. There are two different flow regimes. The mass flow rate is initially linear but approaches an asymptotic value at large blade speeds. The transition point from linear to the asymptotic trend is independent of the gap height. The critical blade spreading speed, above which the mass flow rate is independent on the blade spreading speed, is 0.1 m/s for the system studied here.
- 3) The critical blade spreading speed could be examined by comparing the gravity inertial timescale and spreading inertial timescale, and it is about  $5(gD)^{0.5}$ .

## Acknowledgements

The authors are thankful to DEM Solutions, Edinburgh, UK, for providing a special license for the EDEM software for use in this work. The authors would also like to thank Dr Mehrdad Pasha for his help in facilitating computational work.

## References

- [1] S. Antoniwi, N. McCarthy, E. Pacey, B. Parkin, P. Shelton, Additive manufacturing: opportunities and constraints, *R. Acad. Eng.* (2013) 1–21.
- [2] B. Berman, 3-D printing: the new industrial revolution, *Bus. Horiz.* 55 (2012) 155–162.
- [3] U.M. Dilberoglu, B. Ghahreghapagh, U. Yaman, M. Dolen, The role of additive manufacturing in the Era of industry 4.0, *Procedia Manuf.* 11 (2017) 545–554.
- [4] T. Debroy, H.L. Wei, J.S. Zuback, T. Mukherjee, J.W. Elmer, J.O. Milewski, A.M. Beese, A. Wilson-Heid, A. De, W. Zhang, Additive manufacturing of metallic components – Process, structure and properties, *Prog. Mater. Sci.* 92 (2018) 112–224.
- [5] I. Gibson, D. Rosen, B. Stucker, Additive Manufacturing Technologies, 3D Printing, Rapid Prototyping, and Direct Digital Manufacturing, Springer, New York, 2015.
- [6] W.E. Frazier, Metal additive manufacturing: a review, *J. Mater. Eng. Perform.* 23 (2014) 1917–1928.
- [7] N. Guo, M.C. Leu, Additive manufacturing: technology, applications and research needs, *Front. Mech. Eng.* 8 (2013) 215–243.
- [8] T.D. Ngo, A. Kashani, G. Imbalzano, K.T.Q. Nguyen, D. Hui, Additive manufacturing (3D printing): a review of materials, methods, applications and challenges, *Compos. Part B* 143 (2018) 172–196.
- [9] S.M. Thompson, L. Bian, N. Shamsaei, A. Yadollahi, An overview of direct laser deposition for additive manufacturing; part I: transport phenomena, modeling and diagnostics, *Addit. Manuf.* 8 (2015) 36–62.
- [10] N. Shamsaei, A. Yadollahi, L. Bian, S.M. Thompson, An overview of direct laser deposition for additive manufacturing; Part II: mechanical behavior, process parameter optimization and control, *Addit. Manuf.* 8 (2015) 12–35.
- [11] S. Singh, S. Ramakrishna, R. Singh, Material issues in additive manufacturing: a review, *J. Manuf. Process.* 25 (2017) 185–200.
- [12] S.F. Shirazi, S. Gharekhani, M. Mehrali, H. Yarmand, H.S. Metselaar, N. Adib Kadri, N.A. Osman, A review on powder-based additive manufacturing for tissue engineering: selective laser sintering and inkjet 3D printing, *Sci. Technol. Adv. Mater.* 16 (2015) 033502.
- [13] D.D. Gu, W. Meiners, K. Wissenbach, R. Poprawe, Laser additive manufacturing of metallic components: materials, processes and mechanisms, *Int. Mater. Rev.* 57 (2013) 133–164.
- [14] A. Townsend, N. Senin, L. Blunt, R.K. Leach, J.S. Taylor, Surface texture metrology for metal additive manufacturing: a review, *Precis. Eng.* 46 (2016) 34–47.
- [15] S.A. Khairallah, A.T. Anderson, A. Rubenchik, W.E. King, Laser powder-bed fusion additive manufacturing: Physics of complex melt flow and formation mechanisms of pores, spatter, and denudation zones, *Acta Mater.* 108 (2016) 36–45.
- [16] P. Bidare, R.R.J. Maier, R.J. Beck, J.D. Shephard, A.J. Moore, An open-architecture metal powder bed fusion system for in-situ process measurements, *Addit. Manuf.* 16 (2017) 177–185.
- [17] E.J.R. Parteli, T. Pöschel, Particle-based simulation of powder application in additive manufacturing, *Powder Technol.* 288 (2016) 96–102.

- [18] S. Haeri, Y. Wang, O. Ghita, J. Sun, Discrete element simulation and experimental study of powder spreading process in additive manufacturing, *Powder Technol.* 306 (2016) 45–54.
- [19] H. Chen, Q. Wei, S. Wen, Z. Li, Y. Shi, Flow behavior of powder particles in layering process of selective laser melting: numerical modeling and experimental verification based on discrete element method, *Int. J. Mach. Tools Manuf.* 123 (2017) 146–159.
- [20] S. Haeri, Optimisation of blade type spreaders for powder bed preparation in additive manufacturing using DEM simulations, *Powder Technol.* 321 (2017) 94–104.
- [21] W. Nan, M. Pasha, T. Bonakdar, A. Lopez, U. Zafar, S. Nadimi, M. Ghadiri, Jamming during particle spreading in additive manufacturing, *Powder Technol.* 338 (2018) 253–262.
- [22] P.A. Cundall, O.D.L. Strack, A discrete numerical model for granular assemblies, *Géotechnique* 29 (1979) 47–65.
- [23] C. Thornton, *Granular Dynamics, Contact Mechanics and Particle System Simulations*, Springer, New York, 2015.
- [24] W. Nan, M. Ghadiri, Y. Wang, Analysis of powder rheometry of FT4: effect of particle shape, *Chem. Eng. Sci.* 173 (2017) 374–383.
- [25] J.F. Favier, M.H. Abbaspour-Fard, M. Kremmer, A.O. Razi, Shape representation of axisymmetrical, non-spherical particles in discrete element simulation using multi-element model particles, *Eng. Comput.* 16 (1999) 467–480.
- [26] K. Johnson, K. Kendall, A. Roberts, Surface energy and the contact of elastic solids, *Proc. R. Soc. Lond. A* 324 (1971) 301–313.
- [27] K. To, P.Y. Lai, H.K. Pak, Jamming of granular flow in a two-dimensional hopper, *Phys. Rev. Lett.* 86 (2001) 71–74.
- [28] R.P. Behringer, Dynamics and rheology of cohesive and deformable granular materials, *Jamming and Flow in a Hopper 2007*, pp. 1–3, (IFPRI Report).
- [29] D. Schulze, *Powders and Bulk Solids Behavior, Characterization, Storage and Flow*, Verlag, Springer, Berlin Heidelberg, 2007.
- [30] N.R. M. Statics and Kinematics of Granular Materials, Cambridge University Press, Cambridge, 2005.